SEMARAK ILMU PUBLISHING

Journal of Advanced Research in Applied Sciences and Engineering Technology

Journal homepage:
https://semarakilmu.com.my/journals/index.php/applied_sciences_eng_tech/index
ISSN: 2462-1943

Detection of Kidney Stone and Estimation of its Size using Image Segmentation Techniques

Shraman Jain[1], Rajini G. K.[1], Rahul S. G.[2], Rajkumar R.[2], Velmurugan S.[3,*], M. Jasmine Pemeena priyadarsini[1]

[1] School of Electrical Engineering, Vellore Institute of Technology, Vellore, 632014, Tamil Nadu, India
[2] Department of Electronics and Communication Engineering, Vel Tech Rangarajan Dr. Sagunthala R&D Institute of Science and Technology, 600062 Chennai, India
[3] Department of Biomedical Engineering, Dr. N.G.P. Institute of Technology, 641048 Coimbatore, India

ARTICLE INFO

Article history:
Received 16 August 2023
Received in revised form 1 October 2023
Accepted 23 November 2023
Available online 30 December 2023

Keywords:

Kidney stones; Size; CT; Watershed segmentation

ABSTRACT

The study discusses the development of a reliable strategy for detecting and segmenting kidney stones from CT scans. Kidney stones are solid materials that can form in the kidneys due to excessive amounts of specific minerals in the urine. Severe back, side, lower abdominal, or groin discomfort, or blood in urine can indicate kidney stone presence. The current method for detection using CT scans is widely used, but it requires more precise and efficient technology due to the laborious and time-consuming manual process. The objective of this report is to propose a robust approach for kidney stone detection and segmentation, employing threshold segmentation and the watershed algorithm along with pre-and post-image processing for noise reduction. Additionally, the method estimates the size of the stone, aiding in selecting the appropriate medical procedure for stone removal. The entire process is implemented on a dataset comprising numerous kidney stone images to test and validate its accuracy and reproducibility. The system's image quality enhancement is evaluated by calculating several parameters such as SSIM, PSNR, FSIM, NCC, and NAE on the output images. To further validate the suggested method, a comparison is made with two other existing algorithms based on the mentioned evaluation criteria. The proposed strategy promises to improve the accuracy and reliability of kidney stone detection and segmentation, providing a more efficient and effective solution for medical diagnosis and treatment

1. Introduction

In the modern age, a significant portion of the population leads sedentary lifestyles, which not only impacts overall health but also has adverse effects on kidney health. It becomes crucial to adopt preventive measures from an early age to reduce the occurrence of renal calculi, commonly known as kidney stones. The prevalence of kidney stone-related issues is alarming, with over 500,000 patients seeking emergency medical care annually as per the survey done by National Kidney

* *Corresponding author.*
E-mail address: velmurugan.s@drngpit.ac.in

https://doi.org/10.37934/araset.36.2.91109

Foundation. Disturbingly, one in ten individuals is expected to experience kidney stones at some point in their lives, highlighting the widespread nature of this condition discussed by Oo and Khaing [1]. Moreover, it's important to note that a person may encounter more than one kidney stone throughout their lifetime. If someone has already had one kidney stone, there is a 50% chance of experiencing another one within the next five to seven years. While it may not be possible to eliminate the risk, implementing a few simple yet impactful lifestyle changes can certainly reduce the likelihood of developing kidney stones. In addition to promoting an active lifestyle and regular exercise, maintaining proper hydration levels plays a vital role in kidney stone prevention. Adequate water intake helps dilute the urine and reduces the concentration of minerals that could form into stones discussed by Bahadure *et al.,* [2]. Anitha *et al.,* [3] described a segmentation technique for Alzheimer disease, Moreover, monitoring salt and oxalate intake, both of which are linked to kidney stone formation can be beneficial. Furthermore, dietary modifications, such as increasing the consumption of fruits and vegetables, can enhance kidney health. Certain foods, such as citrus fruits, contain natural compounds that inhibit stone formation. Incorporating these dietary changes can have a positive impact on overall health as well. Kidney stones are solid objects formed from chemicals in the urine, necessitating thorough diagnostic procedures, including imaging tests, physical examinations, and medical history evaluations. Among the imaging options, high-resolution Computerized Tomography (CT) scans are commonly employed for their ability to provide detailed insights into kidney stone characteristics discussed by Abdallah and Alqahtani [4]. Cui *et al.,* [5] explained that size of kidney stones can vary significantly, ranging from as small as a grain of sand to as large as a pebble or even a golf ball. Typically, larger stones result in more noticeable symptoms. Smaller kidney stones can often be passed naturally without medical intervention, while larger stones may require various treatments, such as ureteroscopy, shockwave lithotripsy, percutaneous nephrolithotomy, or nephrolithotripsy. Dhage *et al.,* [6] discussed that the presence of kidney stones can lead to a range of distressing symptoms, including severe lower back pain, blood in the urine (haematuria), nausea, vomiting, fever, chills, and changes in urine appearance or odour. If left untreated, kidney stones can give rise to Urinary Tract Infections (UTIs), including kidney infections, and may lead to a potential loss of kidney function. Dhankhar *et al.,* [7] discussed that in the medical sector, image processing plays a critical role, especially in medical image processing, which involves analysing image datasets acquired from CT or Magnetic Resonance Imaging (MRI) scanners. Dhiman *et al.,* [8] discussed the MRI scanning process enables the identification of various pathologies, facilitates surgical planning, and supports research endeavours. Medical professionals, including radiologists, engineers, and doctors, utilize image processing to gain valuable insights into the anatomical structures of specific individuals or populations. One of the primary advantages of medical image processing lies in its ability to conduct in-depth, non-invasive investigations of internal anatomy. This capability has become a cornerstone of advancements in medicine in recent years. With ever-improving image quality and state-of-the-art software tools, accurate digital reconstructions of anatomical structures, such as bones and soft tissues, can be achieved at various scales, contributing to improved diagnostic accuracy and treatment planning. As medical image processing continues to evolve and integrate with emerging technologies like machine learning and artificial intelligence, its potential for transforming kidney stone diagnosis and treatment becomes even more promising stated by Ding *et al.,* [9].

Hagler Jr *et al.,* [10] studied and stated that Image segmentation is a widely used technique in digital image processing and analysis, aimed at partitioning an image into multiple segments or regions, often based on specific pixel properties. This process involves distinguishing the foreground from the background or grouping pixels with similar colour or shape attributes. For instance, in medical imaging, image segmentation plays a crucial role in identifying and categorizing pixels or

voxels (3D volume elements) corresponding to tumours in the brain or other organs of patients by Hore and Ziou [11]. Early detection and accurate size measurement of kidney stones are essential for effective treatment and reducing the risk of developing severe kidney stone disease. Utilizing abdominal CT scans, automated systems can aid in detection, eliminating the need for manual stone diameter/area measurement, thereby lightening the workload for medical professionals presented by Hou *et al.,* [12]. The objective of this study is to develop a kidney stone diagnosis tool that automates the detection process. The proposed algorithm is based on threshold segmentation and the watershed algorithm, allowing for the identification of the stone area in a CT image with precision and accuracy. By minimizing manual intervention, the algorithm enables efficient detection of kidney stones and provides an estimation of their size. This automation enhances diagnostic efficiency and supports early intervention strategies, ultimately improving patient outcomes and alleviating the burden on healthcare professionals studied by Vineela *et al.,* [13] employed ultrasound images to detect kidney stones. Ultrasound images often contain speckle noise, making it challenging for human observers to eliminate the noise. In their study, the authors opted for the median filter over the Gabor filter for automatic kidney stone detection in ultrasound images. The proposed methodology involved pre-processing and segmentation of the ultrasound image, followed by morphological analysis, to identify the presence of kidney stones. The generated image was then utilized to precisely locate each stone, and an edge detection approach was applied to determine the stones' structure and shape. The integration of these three techniques resulted in an effective method for kidney stone detection. The accuracy of the suggested algorithm was reported to be 92.57%, a commendable achievement when compared to previous algorithms. Rajput *et al.,* [14] emphasize the crucial importance of accurately locating urinary calculus before performing surgery. Due to the presence of speckle noise in ultrasound images, manual detection of kidney stones is challenging; hence, automated algorithms are necessary. This research proposes a method for automatically identifying kidney stones without human intervention, eliminating the need for manual investigation. The results section presents parameter values that demonstrate the feasibility and applicability of the proposed method for computer-aided kidney stone detection diagnosis. Even ultrasound images require additional pre-processing, such as the removal of speckle noise and subsequent segmentation and processing, to ensure accurate detection. The study addresses these challenges, aiming to improve the accuracy and efficiency of kidney stone detection in ultrasound images. In their proposed study, Akkasaligar *et al.,* [15] utilize the level-set segmentation method to detect kidney stones. The first step involves segmenting regions of interest and preprocessing the input photos. The level set segmentation proves to be a successful solution for accurately addressing the segmentation problem. CT scans are powerful diagnostic tools with various applications. They employ X-rays to create detailed images of the body's internal structures in thin slices, which are then digitally stored. During the CT scan preparation, the input image is cropped. Subsequently, the level-set segmentation approach is employed to segment the input image. By examining the segmented images, the study can determine the size and location of the kidney stones accurately. The level-set segmentation method plays a pivotal role in achieving precise and reliable kidney stone detection from CT scans Cui *et al.,* [16] used three sets of abdominal Non-Contrast Computed Tomography (NCCT) images: a segmentation dataset (n=167), a hydronephrosis classification dataset (n=282), and a test dataset (n=117). Their model consisted of four steps: kidney and renal sinus segmentation using 3D U-Nets, hydronephrosis grading using deep 3D dual-path networks, kidney stone detection and segmentation using thresholding, and determining the stone's location. The stone detection algorithm achieved 95.9% sensitivity and 98.7% PPV. The hydronephrosis classification algorithm had an AUC of 0.97. The scoring model for stone size, tract length, and essence grade closely matched radiologists' assessments (correlation coefficients of 0.95, 0.97, and 0.97, respectively) Thein *et al.,*

[17] tackle the challenge of accurate kidney stone segmentation from CT images, where variations in size and shape complicate the 3D organ segmentation method. To aid segmentation, a reader-independent preprocessing technique was developed. Three thresholding algorithms were employed to remove unwanted regions (soft organs, bone skeletons, and bed mats). The approach achieved 95.24% sensitivity, improving detection and reducing noise. Although effective, the method relies on past image information, making it less resilient. Elton *et al.,* [18] developed a deep learning-based solution for kidney stone detection using abdominal NCCT scans. The system achieved a sensitivity of 0.86 with 0.5 false positives per image on a challenging test set. The correlation with manual measurements was strong (r2 = 0.95), and an external validation set achieved an area under the receiver operating characteristic of 0.95. However, false positive results were observed due to small atherosclerotic plaques in the renal sinus studied by Elton *et al.,* [18]. In their study, Hasan and Ahmad [19] employed trilateral filters as preprocessing techniques followed by a median filter. The pre-processed image was then used for watershed segmentation. The authors propose that these preprocessing techniques can address the issue of over-segmentation by the watershed algorithm by reducing detailed texture through smoothing. Additionally, these techniques aid in noise reduction using a median filter, image sharpening based on a Gaussian high pass filter, and contrast enhancement. Tarhini and Shbib [20] argue that MRI scans are superior to CT scans in diagnosing tumours due to their ability to create more accurate images and detect small or hard-to-detect tumours effectively. Developing automated systems for quick and precise brain tumour detection involves combining various technologies. Their proposed method involves threshold segmentation and watershed segmentation to highlight the tumour site, followed by post-processing with morphological operators to enhance image quality. To create such systems, researchers have explored machine learning, deep learning, image processing, and convolutional neural networks. In their study, Khan *et al.,* [21] utilized a Gaussian filter to enhance the gamma contrast. They employ watershed segmentation to extract features from tumour images and subsequently apply post-processing methods like Maximally Stable Extremal Region (MSER) and Histogram Oriented Gradients (HOG) to eliminate any remaining extraneous characteristics. Feature selection is performed using the chi-square distance. In their research, references Seere and Karibasappa [22] perform image pre-processing using a combination of the median filter, contrast enhancement, and stationary wavelet method. The segmentation process involves two steps: first, threshold segmentation is used to group pixels with similar intensities, followed by watershed segmentation. For tumour classification after segmentation, they suggest employing Support Vector Machine (SVM), a supervised machine-learning method. Following watershed segmentation, Jemimma and Vetharaj [23] employ Dynamic Angle Projection Pattern (DAPP) as a post-processing technique. The 5x5 mask used in this method rotates the central pixel value by 45 degrees compared to the surrounding pixels. By combining this masked image with the watershed segmentation result, the pixel intensity is binarized, allowing texture interpretation due to decimal encoding of the values. For tumour classification, the convolutional neural network (CNN) utilizes the pooling layer and the convolution layer in the later stages. The study performed by Mehmet Baygin *et al.,* [24] highlights a novel ExDark19 model for automated kidney stone detection in CT images. Achieving over 99% accuracy using two validation methods, this automated system shows promise in reducing human error during kidney stone screenings by urologists. The literature review in this chat provides an overview of different research papers focused on the detection of kidney stones and brain tumours from medical images. The studies employ various techniques, such as ultrasound image processing, CT scan analysis, and deep learning methods [25-27]. The literature review highlights several critical research gaps in the domain of kidney stone detection through CT imaging. Mohit *et al.,* [28] conducted several studies related to kidney stone estimations [28-30]. Firstly, there is a notable need to automate the detection of smaller

kidney stones. Standardization of datasets and evaluation metrics is lacking, hindering fair comparisons and benchmarking. Additionally, integrating clinical context, enhancing real-time processing, and ensuring generalizability to diverse populations are pressing challenges. Bridging these gaps will significantly advance automated kidney stone detection, making it more accurate, efficient, and clinically relevant.

2. Materials and Methods

The methodology focuses on stone detection using thresholding and watershed segmentation techniques. While these approaches have their advantages, the combination of pre-processing and post-processing methods plays a crucial role in enhancing output accuracy by addressing the limitations of individual techniques. The approach involves several pre-processing techniques, including grayscale conversion, noise reduction using median and top hat filters, image smoothing, contrast enhancement, image binarization, morphological erosion, and morphological dilation. These pre-processing methods contribute to improved results for thresholding and watershed segmentation in stone identification. Additionally, post-processing methods like k-means clustering and binary masking are applied to further refine the results.

2.1 Preprocessing Stage

The proposed algorithm takes a CT scan as input. The colour scheme of the image is verified, and if it is in a different colour scheme, the image is converted to a grayscale. Figure 1 illustrates the input CT image and the resulting grayscale image with the kidneys highlighted.

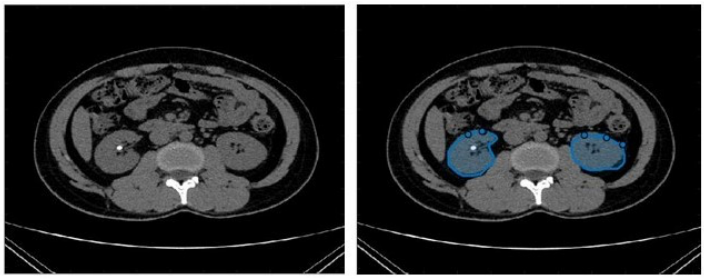

Fig. 1. (a)Input CT image (b) grayscale image with kidneys highlighted

The grayscale image undergoes a median filter, which eliminates noise by calculating the median value of a 9-pixel window. After that, a 2x7 smoothing matrix is used for image smoothing, where one row consists of 1s and the other row of 0s. The smoothing process acts as an average filter, averaging out pixel values as the smoothing matrix moves through each window. The resulting output matrix is compatible with the subsequent smoothing function due to zero padding provided by the 0s in the matrix. Figure 2 illustrates the process with the kidneys isolated from the abdominal CT image, followed by the isolated kidneys after applying the median filter and image smoothing.

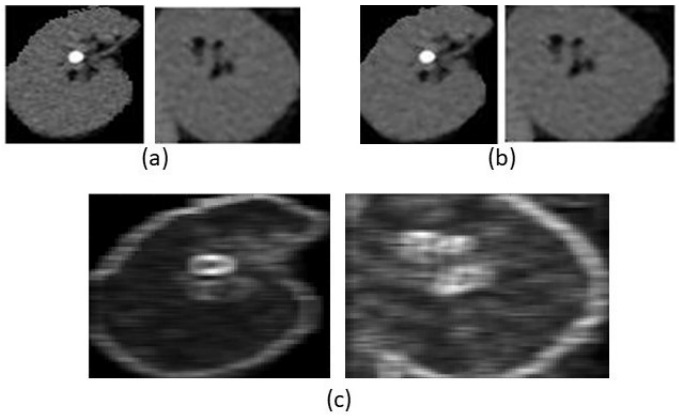

Fig. 2. (a) Isolated kidneys (b) Image after the median filter (c) Image after smoothing

Following the smoothing process, the image undergoes a top hat filter application to remove noise from the foreground. The top 1% and bottom 1% of pixel intensity values are saturated to enhance contrast. The resulting improved image then goes through image binarization, where each pixel's intensity is compared to a pre-defined threshold value. The transformation results in a binary image, with pixel values of 1 for intensities exceeding the threshold and 0 for intensities below the threshold. This produces a black-and-white image, with black represented as 1 and white as 0 in the binarized matrix. Morphological erosion is applied to refine the image boundaries by removing any excess pixels from the outer edges. On the other hand, morphological dilation is used to fill in any gaps or holes in the image caused by noise, thereby enhancing the overall image quality. Figure 3 displays the kidney's image after the application of a top-hat filter, contrast enhancement, binarization, and morphological operations as part of the pre-processing techniques.

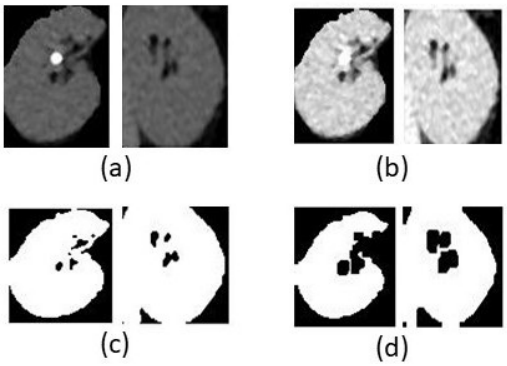

Fig. 3. (a) Image after top-hat filter (b) Image after contrast enhancement (c) Image after binarization (d) Image after morphological operations

2.2 Processing Stage and Watershed Algorithm

The threshold algorithm is then applied to the pre-processed image. It determines a threshold value based on the average intensity values of the pixels in the image. Pixels with intensities above the threshold value are set to one, while those below it is set to zero. The resulting image after thresholding is then complemented before being used for watershed segmentation. The watershed algorithm effectively segments the image into distinct regions or objects based on their intensity or gradient characteristics, utilizing marker points for guidance. It is a valuable tool in computer vision and image

processing for various applications requiring accurate image segmentation. The watershed algorithm is depicted as follows,

2.2.1 Compute the gradient magnitude of the image

- $G(x, y) = \nabla I(x, y) = [\partial I/\partial x, \partial I/\partial y]$: Calculate the gradient of the image to obtain the magnitude of the gradient at each pixel location.

2.2.2 Generate the watershed segmentation map

- Initialize a label matrix L(x, y) to store the segmentation result. Set all pixels in L to an initial value (e.g., -1).
- Assign unique labels to the marker points (e.g., 0, 1, 2, ...).
- For each unlabelled pixel (x, y) in the image: a. Find neighbouring labelled pixels. b. If there is only one unique label among the neighbours, assign that label to the current pixel (x, y). c. If there are multiple unique labels among the neighbours, mark the current pixel (x, y) as a watershed point.
- Repeat the process until all pixels have been labelled

2.2.3 Resolve watershed regions

- For each watershed point, check neighbouring pixels and assign the label of the nearest marker point to the watershed point

In watershed segmentation, the entire image matrix is treated as the watershed area, with the image regions acting as catchment basins and the edges of image objects acting as ridge lines. The pixel intensities are classified based on the local maxima obtained through watershed segmentation. Figure 4 illustrates the image of kidneys after undergoing the processing stage, including thresholding, complementing the thresholding, and watershed segmentation techniques.

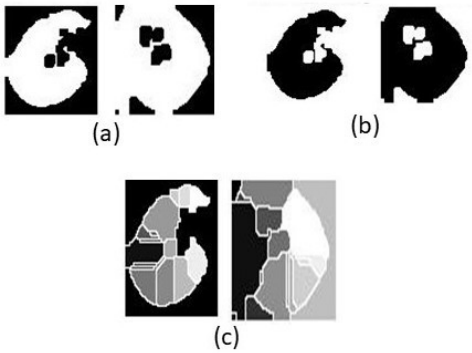

Fig. 4. (a) Image post thresholding (b) Complement of image (c) Image after watershed segmentation

2.3 Post Processing Stage

Following segmentation, post-processing techniques are implemented on the image. The image is partitioned into 'k' distinct clusters using k-means clustering, where 'k' is set to 4 for this particular

process. Clustering is performed by assigning each pixel to the closest centroid among the 'k' centroids. This results in four layers of the image, each representing a different grouping of pixels from the centroids. Figure 5 displays the superimposed k-means clustering image of both kidneys, while Figure 6 illustrates the four layers obtained from the k-means clustering of both kidneys.

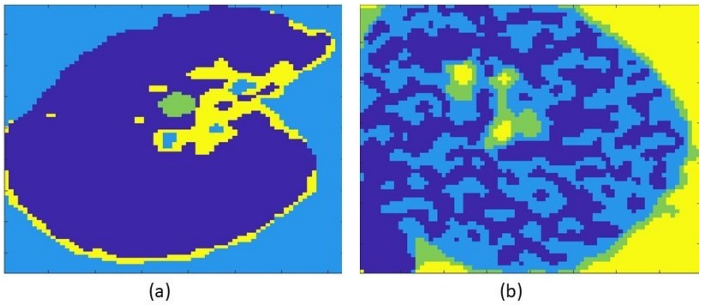

Fig. 5. Superimposed k-means clustering (a) left kidney (b) right kidney

The resulting complete image is formed by combining these four layers. Subsequently, a binary mask is applied to perform feature extraction. This binary mask defines the Region of Interest (ROI) in the image, where pixels with a value of 1 represent ROI-related pixels, and pixels with a value of 0 represent background pixels.

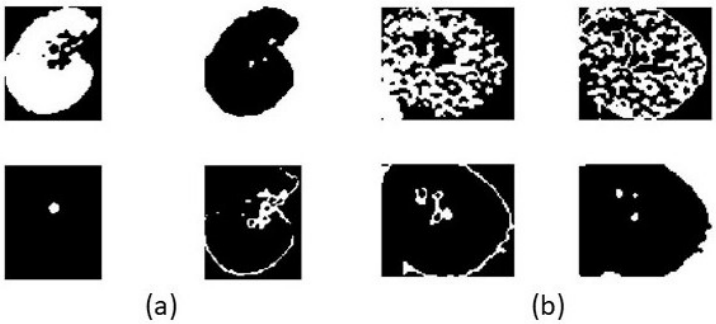

Fig. 6. Four layers of k-means clustering of (a) left kidney (b)right kidney

Figure 7 illustrates the image of kidneys after binary masking. The proposed method efficiently detects and segments kidney stones from the CT scan, highlighting their locations. Moreover, it accurately determines and displays the size of the detected stones. The emphasis is placed on extensive pre-processing techniques to eliminate unwanted noise from the image.

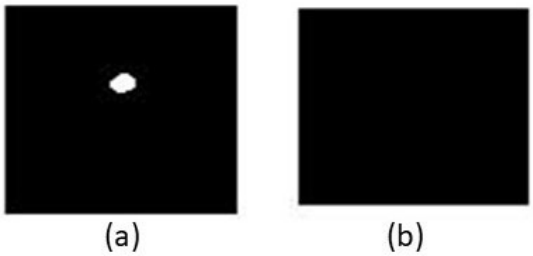

Fig. 7. Image after binary masking (a) left kidney (b) right kidney

2.4 Size of Kidney stone

The length of the major axis and surface area of the detected stone(s) are also computed. These parameters are initially calculated in terms of pixels and then converted to millimetres using the following formula shown in Eq. (1)

$$1 \text{ pixel} = 0.2645833333 \text{ mm} \quad (1)$$

The classification of stone size in terms of chances of passing naturally, the time required to pass and possible treatments is obtained from Meddo Health and given in Table 1.

Table 1
Classification of stone size in terms of chances of passing naturally

Kidney stone size	Percentage of natural passage	Time required for natural passage (average)	Method of treatment
Less than 2 mm	80%	8 days	Home remedies
2 to 4 mm	80%	12 days	Home remedies
4 mm	80%	31 days	Home remedies
4 to 7 mm	60%	45 days	Home remedies
Larger than 7 mm	20%	12 months	Ureteroscopy
1 to 2 cm	Cannot pass	-	Lithotripsy
Larger than 2 cm	Cannot pass	-	Percutaneous nephrolithotomy

2.5 Performance Evaluation Metrics

The algorithm's effectiveness in terms of image quality is assessed using various metrics. The evaluation aims to understand the algorithm's performance with different image categories and determine optimal parameters for various applications. Six measures, namely Structure Similarity Index Measure (SSIM), Peak Signal-to-Noise Ratio (PSNR), Entropy, Feature Similarity Index Measure (FSIM), Normalized Cross Correlation (NCC), and Normalized Absolute Error (NAE), are utilized to evaluate a set of images.

2.5.1 SSIM

This normalized measure is used to assess the similarity between the input and processed images, considering structure, contrast, and luminance as comparison criteria. SSIM as shown in Eq. (2) and Eq. (3) measures the level of image degradation caused by preprocessing. It groups pixels in the processed reference image based on their similar pixel densities. FSIM is similar to SSIM but contrasts minor characteristics, using phase congruency and gradient magnitude as comparison criteria.

$$SSIM(x,y) = \frac{(2\mu_x\mu_y+c_1)(2\sigma_{xy}+c_2)}{(\mu_x^2+\mu_y^2+c_1)(\sigma_x^2+\sigma_y^2+c_2)} \quad (2)$$

Where, $\mu_x, \mu_y \; are \; mean \; of \; x\&y$, $\sigma_x, \sigma_y - variance \;\; of \; x\&y$ and $\sigma_{xy} - cross \; correlation \; of \; x\&y$ respectively.

$$S_L(x) = [S_{PC}(x)]^{\alpha}[S_G(x)]^{\beta} \quad (3)$$

The parameters α and β are utilized to adjust the relative significance of PC (phase congruency) and GM (gradient magnitude) features, while 'SPC' and 'SG' represent the similarities based on phase congruency and gradient magnitude, respectively.

2.5.2 FSIM

FSIM is employed to evaluate image quality. It compares features of the two images based on changes in light intensity and changes in intensity in a specific direction.

2.5.3 PSNR

PSNR is the ratio of the signal's power to the power of noise that distorts the signal which is denoted in Eq. (4). As PSNR increases, the amount of noise causing distortion decreases. PSNR takes advantage of the Mean Squared Error (MSE) between the input and reference images, as well as the image data type range.

$$PSNR = 10\ log_{10}\left(\frac{255^2}{MSE}\right) \text{(dB)} \tag{4}$$

Where 'MSE' is the mean square error and 'R' is the maximum fluctuation in the input image.

2.5.4 Entropy

Entropy quantifies the texture of the image, revealing the amount of information it contains. It converts the pixel intensity values into a width-based numerical parameter.

2.5.5 NCC

NCC is employed for template matching, aiming to find occurrences of the original image in the modified image as denoted in Eq. (5). It measures the similarity between two images by calculating cross-correlation values window by window through the reference and processed images.

$$NCC = \frac{\sum_{i=1}^{m}\sum_{j=1}^{n}(|A_{ij}\ X\ B_{ij}|)}{A_{ij}^2} \tag{5}$$

Where, m x n is the dimension and A and B are, respectively, the reference image and processed image pixel values.

2.5.6 NAE

NAE measures the variation between the original and the processed image by indicating the difference in numbers between the two photos as denoted in Eq. (6). The precise difference between the processed and reference images is measured by NAE.

$$NAE = \frac{\sum_{i=1}^{m}\sum_{j=1}^{n}(|A_{ij}-B_{ij}|)}{\sum_{i=1}^{m}\sum_{j=1}^{n}(A_{ij}|)} \tag{6}$$

where, for a given size of m x n, A and B are the respective image pixel values of the reference picture and processed image.

3. Results

The project aims to identify kidney stones and estimate their size from abdominal CT scans using image processing techniques. The main focus is on thresholding and watershed segmentation, along with various pre- and post-processing algorithms to address the issue of over-segmentation, a common drawback of the watershed algorithm. The results obtained are evaluated and compared with other similar algorithms using various statistical parameters. The algorithm is tested on more than 150 images from an open-source dataset, Kaggle. The Kaggle Kidney Stone Images Dataset is a collection of medical images showcasing kidney stones obtained from the Kaggle platform. These images provide visual insights into kidney stones, aiding research and analysis in the field of urology and medical imaging. The findings on ten randomly selected images are presented in the figures below. These images vary in terms of stone size, number, and scan quality, and are chosen without any specific pattern.

3.1 Kidney Stone Detection and Size Estimation

Figures 8 to 12 showcase the results of our proposed methodology for kidney stone detection and size estimation from abdominal CT scans. In these figures, the images of both kidneys are presented, with the identified kidney stones highlighted. The left side of each image displays the input after isolating both kidneys from the original abdominal CT scan. On the right side of the image, the detected kidney stone(s) and their corresponding sizes are observed after applying the proposed methodology. The size of the kidney stone(s) is measured and presented in two ways: the length of the major axis in millimetres (mm) and the area of the stone in square millimetres (mm²). This information is crucial for proper diagnosis and treatment planning, as the size of the stone(s) plays a significant role in determining the appropriate medical intervention. Our methodology effectively segments and identifies kidney stones, providing accurate information about their size and location. This automated approach eliminates the need for manual intervention in stone detection, reducing human errors and improving efficiency. The combination of thresholding, watershed segmentation, and various pre- and post-processing techniques ensures the accuracy and reliability of the results.

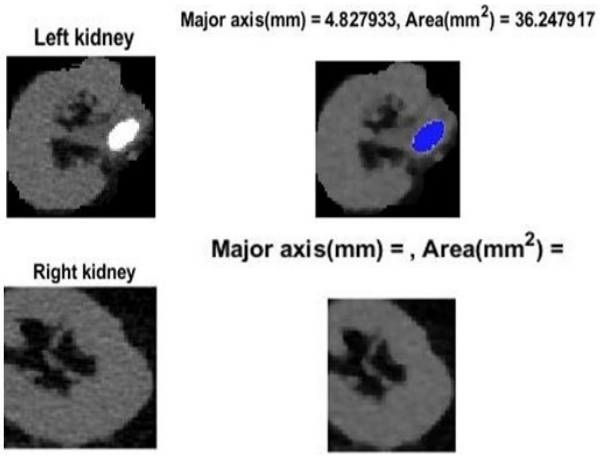

Fig. 8. Presence of Kidney stones in sample 1

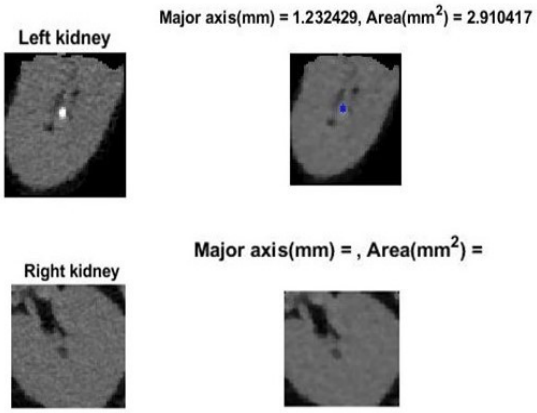

Fig. 9. Presence of Kidney stones in sample 2

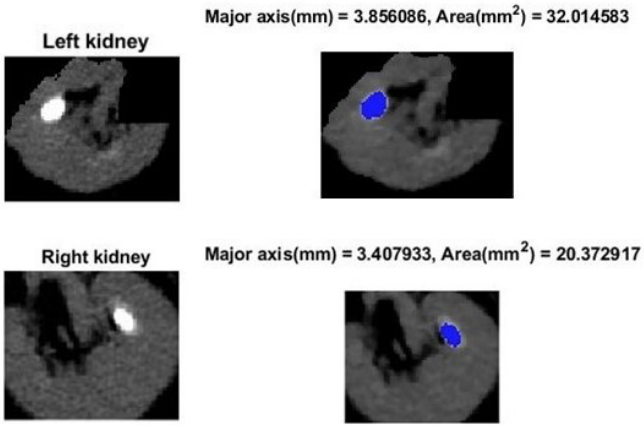

Fig. 10. Presence of Kidney stones in sample 3

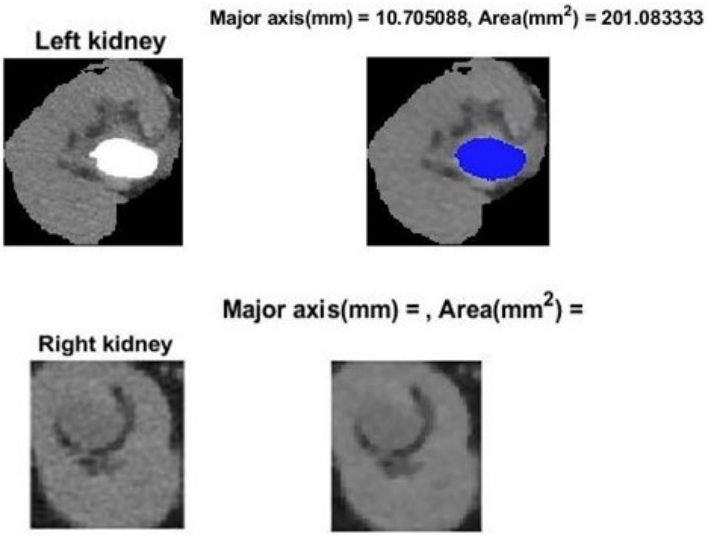

Fig. 11. Presence of Kidney stones in sample 4

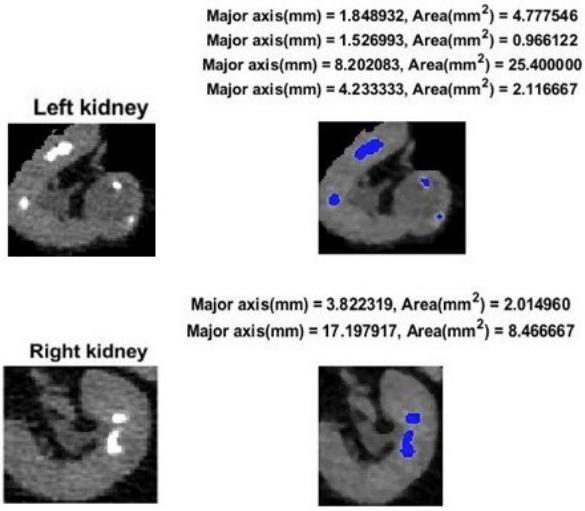

Fig. 12. Presence of Kidney stones in sample 5

Irrespective of the variations in size, number, or contrast level in the CT scan images, our algorithm consistently and accurately identifies the presence of kidney stone(s). This achievement can be attributed to the combination of pre-processing and post-processing techniques, along with the main components of thresholding and watershed segmentation, which significantly contribute to the approach's overall accuracy and performance.

3.2 Measure of Performance Evaluation Metrics

A sample of 15 images was selected from the dataset to evaluate the algorithm's performance parameters regarding image quality. The results of this evaluation are presented in Table 2, Table 3 and Figure 13. These performance parameters play a crucial role in determining the accuracy and effectiveness of the proposed algorithm in detecting and estimating the size of kidney stones from abdominal CT scans. The assessment of image quality is vital in ensuring the reliability and precision of the algorithm's output. By analysing the data from these sample images, valuable insights can be gained into the algorithm's performance and its ability to accurately detect kidney stones and estimate their size.

Table 2
Statistical analysis of the left kidney

Image	SSIM	PSNR	FSIM	Entropy	NCC	NAE	Area(mm^2)	Major axis length (mm)
1	0.915	31.056	0.955	4.950	0.988	0.045	12.700	2.221
2	0.918	33.435	0.961	5.057	0.992	0.042	0.000	0.000
3	0.880	30.298	0.946	4.186	0.990	0.052	1.852	1.026
4	0.905	31.284	0.942	4.634	0.991	0.060	0.000	0.000
5	0.891	29.537	0.950	4.158	0.988	0.054	1.587, 12.700	1.013, 2.481
6	0.813	30.210	0.935	4.548	0.967	0.093	0.000	0.000
7	0.911	32.852	0.951	5.152	0.996	0.030	201.083	10.705
8	0.903	31.153	0.952	5.190	0.993	0.051	12.170, 9.789	2.280, 2.206
9	0.913	27.865	0.946	4.419	0.985	0.059	20.902, 1.323	3.634, 0.736

10	0.935	30.149	0.950	4.029	0.991	0.052	8.202, 25.400, 4.233, 2.117	1.849, 4.777, 1.527, 0.966
11	0.862	29.551	0.953	4.303	0.985	0.059	2.910	1.232
12	0.894	30.504	0.944	4.593	0.987	0.063	5.292	1.646
13	0.923	33.257	0.954	4.538	0.993	0.052	32.015	3.856
14	0.914	31.941	0.968	4.650	0.990	0.042	5.821	1.658
15	0.894	32.648	0.947	5.220	0.994	0.058	36.248	4.828

Table 3
Statistical analysis for right kidney

Image	SSIM	PSNR	FSIM	Entropy	NCC	NAE	Area(mm^2)	Major axis length (mm)
1	0.892	34.172	0.956	5.596	0.986	0.038	0.000	0.000
2	0.891	33.624	0.953	5.918	0.990	0.044	1.852	0.856
3	0.815	30.683	0.932	5.816	0.984	0.053	1.323, 0.530	0.735, 0.611
4	0.884	30.536	0.934	6.765	0.988	0.057	6.350, 0.794, 13.758, 1.323, 10.583	1.638, 0.683, 2.644, 0.736, 2.092
5	0.818	32.004	0.933	5.917	0.988	0.055	11.906	2.507
6	0.855	32.245	0.957	4.650	0.983	0.081	6.350	1.638
7	0.883	32.394	0.950	6.097	0.985	0.036	0.000	0.000
8	0.865	30.654	0.935	6.368	0.988	0.056	5.821	1.658
9	0.873	31.777	0.937	6.550	0.989	0.053	11.113	2.436
10	0.881	30.681	0.931	6.780	0.989	0.065	17.198, 8.466	3.822, 2.014
11	0.812	31.885	0.929	5.379	0.977	0.049	0.000	0.000
12	0.843	32.114	0.927	6.020	0.988	0.068	0.000	0.000
13	0.900	34.401	0.956	5.352	0.993	0.053	20.373	3.408
14	0.882	34.010	0.953	5.253	0.978	0.037	0.000	0.000
15	0.831	31.606	0.917	5.926	0.986	0.068	0.000	0.000

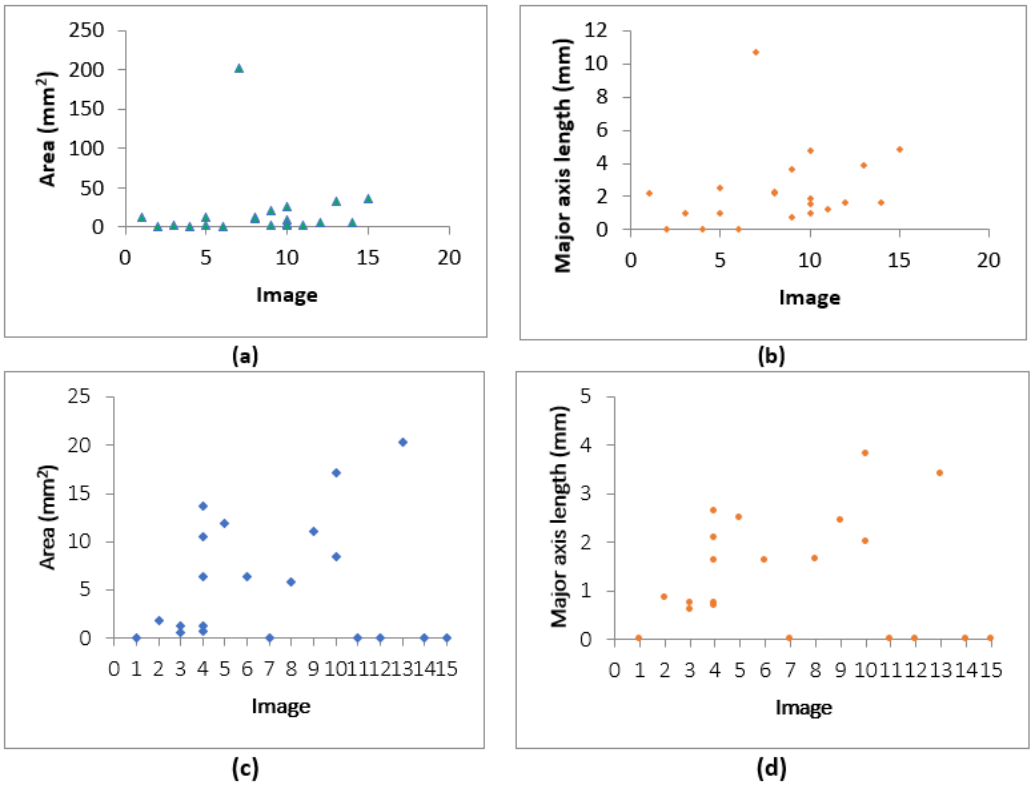

Fig. 13. (a) Image Vs Area (mm2) of left kidney (b) Image Vs Major axis length (mm) of left kidney (c) Image Vs Area (mm2) of right kidney (d) Image Vs Major axis length (mm) of right kidney

The proposed algorithm for kidney stone detection and size estimation from abdominal CT scans is evaluated using various image quality measures. The results from Table 2 and Table 3 demonstrate the algorithm's effectiveness and accuracy in identifying kidney stones and estimating their size.

i. SSIM (Structural Similarity Index Measure): The SSIM values range from 0.907 to 0.935, with the highest value of 0.935 for Image 10 of the left kidney. These high SSIM values indicate that the modified images retain their structural identity.
ii. PSNR (Peak Signal-to-Noise Ratio): The PSNR values range from 1.090 to 34.401, with the highest value of 34.401 for Image 13 of the right kidney. These high PSNR values suggest that the strength of the signal is much stronger than the noise's ability to obscure it.
iii. FSIM (Feature Similarity Index Measure): The FSIM values range from 0.949 to 0.968, with the highest value of 0.968 for Image 14 of the left kidney. These high FSIM values indicate better outcomes, considering phase congruency and gradient magnitude for assessing minor features.
iv. Entropy: The entropy values range from 4.558 to 6.780, with the highest value of 6.780 for Image 10 of the right kidney. These results indicate that the images contain a significant amount of information.

The NCC parameter is used for template matching, and the highest NCC value of 0.996 is observed for Image 7 of the left kidney, indicating a strong match. The NAE values range from 0.030 to 0.196, with the lowest value of 0.030 for Image 7 of the left kidney, indicating good image quality. Tables 2 and 3 and Figure 13 present results based on a subset of 15 images from the dataset. The mentioned subset serves as a representative sample for detailed analysis. However, it's important to note that

the methods were initially tested on a more extensive dataset comprising over 150 images. Later, for comprehensive statistical evaluation, the statistical metrics were calculated using the broader dataset. The average SSIM value was 0.899, the average PSNR value was 32.049, the average FSIM value was 0.959, and the average entropy value was 4.989. Additionally, the normalised cross-correlation was found to be 0.988, and the normalised absolute error was 0.0580. These results demonstrate the algorithm's effectiveness in accurately detecting kidney stones and estimating their size from abdominal CT scans. Overall, the high values of SSIM, PSNR, FSIM, and entropy, along with the low NAE value, indicate that the proposed algorithm produces reliable and informative results for kidney stone detection and size estimation.

3.2 Comparative Analysis

In the proposed algorithm, the input image undergoes several pre-processing steps. First, a median filter is applied, followed by image smoothing. Next, the Top-Hat filter is used to process the image, and its contrast is increased to reduce noise. Morphological erosion and dilation are then applied to further enhance the image's quality. After these pre-processing steps, thresholding and watershed segmentation are performed. Subsequently, K-means clustering and binary masking techniques are utilized to precisely identify and emphasize the kidney stone area. Comparative analysis is presented in Table 4.

Table 4
Comparative analysis

Approaches	SSIM	PSNR	FSIM	Entropy	NCC	NAE
Proposed algorithm (avg. of both kidney images)	0.863	30.637	0.934	5.429	0.988	0.064
Vineela *et al.,* [13]	0.044	7.764	0.695	0.269	0.352	5.243
N. Thein *et al.,* [17]	0.570	14.604	0.609	1.581	0.320	1.022

This approach is compared to two other algorithms that are currently in use. These alternative algorithms differ in their pre-and post-processing methods, which are combined with thresholding and watershed segmentation. Vineela *et al.,* proposed a method specifically tailored for kidney stone detection utilizing various image processing techniques on ultrasound images. In their study, pre-processing involved procedures such as applying a median filter, contrast enhancement, and edge filtering. The segmentation was achieved using K-means clustering, followed by morphological operations for post-processing. Conversely, Thein *et al.,* focused-on kidney stone detection, employing a different approach altogether. The output images from all three methods are evaluated using different parameters, and the results show significant differences due to the variations in pre-processing and post-processing stages. A comparative analysis of the proposed algorithm with two other existing methods [13,17] is presented in Table 4 which shows the evaluation metrics for all three algorithms. The SSIM and FSIM values of the suggested algorithm are 0.863 and 0.934, respectively, which significantly outperform the values of the other two references. These higher values demonstrate the superior processing capabilities of the suggested method. Additionally, the suggested algorithm achieves a PSNR value of 30.637, noticeably higher than the other two algorithms, indicating that the algorithm effectively maintains the image's quality. Furthermore, the suggested algorithm exhibits an entropy value of 5.429, significantly higher than the entropy values of the other two references, as evident from the table. This result indicates that the proposed approach preserves the most information when compared to images processed using the other methods under consideration. Moreover, the NCC value of the suggested approach is 0.988,

significantly higher than the values obtained from the other two algorithms. Conversely, the low NCC values for the other two references suggest high distortion in the processed images. The proposed algorithm also achieves the lowest NAE value of 0.064, slightly lower than the value obtained from the reference [8]. This result further demonstrates the accuracy and efficiency of the suggested approach in maintaining image fidelity. In summary, the proposed algorithm outperforms the other two methods in all evaluation metrics, indicating that it carefully processes the images while preserving their originality, giving it a clear advantage over the alternative approaches.

4. Conclusions

In recent times, the application of CT scans in medical research has witnessed substantial growth, accompanied by increasing demand for automation systems and tasks. This study aimed to accurately identify kidney stones in CT images and determine their size with minimal manual intervention, employing a two-stage process. The initial stage involved essential pre-processing methods, encompassing the implementation of the median filter, top-hat filter, morphological erosion, and dilation. These techniques effectively eliminated unwanted noise from the image, leading to an enhancement in overall image quality. In the subsequent stage, the pre-processed image underwent segmentation through the thresholding and watershed segmentation method, based on pixel intensity levels. For feature extraction, post-processing techniques, including K-means clustering and binary masking, were utilized. To validate the accuracy and reproducibility of the proposed method, it was tested on a dataset containing numerous CT scans of the abdominal region with kidney stones. The system's performance was evaluated through performance metrics applied to the output images. The results demonstrated the efficiency of the algorithm in accurately processing images and detecting kidney stones. In future applications, the potential for expanding the approach lies in the integration of deep learning, machine learning, or neural networks. Training the dataset using these techniques could enhance the algorithm's capabilities, leveraging dynamic data and reducing the need for human intervention, ultimately improving the sensitivity and accuracy of the results by identifying specific patterns or sequences. Furthermore, exploring diverse combinations of more intricate pre- and post-processing algorithms is anticipated to further enhance the quality of the results. Image processing remains a highly sought-after tool for future medical research, owing to its versatility and accuracy in handling complex medical data. In summary, the proposed algorithm effectively addresses the challenges associated with kidney stone detection and size estimation in CT images. The amalgamation of pre-processing techniques, thresholding, and watershed segmentation demonstrates efficacy in achieving reliable and informative results. As the field of medical imaging continues to advance, this approach opens up possibilities for further improvements and advancements in the diagnosis and treatment of kidney stones and other medical conditions.

Acknowledgements

The administration of Vellore Institute of Technology, Vellore, India supplied computing resources for the completion of this study, and the authors are appreciative of their assistance.

References

[1] Oo, Swe Zin, and Aung Soe Khaing. "Brain tumor detection and segmentation using watershed segmentation and morphological operation." *International Journal of Research in Engineering and Technology* 3, no. 03 (2014): 367-374. https://doi.org/10.15623/ijret.2014.0303068

[2] Bahadure, Nilesh Bhaskarrao, Arun Kumar Ray, and Har Pal Thethi. "Image analysis for MRI based brain tumor detection and feature extraction using biologically inspired BWT and SVM." *International journal of biomedical imaging* 2017 (2017). https://doi.org/10.1155/2017/9749108

[3] Anitha, R., and S. Jyothi. "A segmentation technique to detect the Alzheimer's disease using image processing." In *2016 International Conference on Electrical, Electronics, and Optimization Techniques (ICEEOT)*, pp. 3800-3801. IEEE, 2016. https://doi.org/10.1109/ICEEOT.2016.7755424
[4] Abdallah, Yousif Mohamed Y., and Tariq Alqahtani. "Research in medical imaging using image processing techniques." *Medical Imaging-Principles and Applications* 10 (2019). https://doi.org/10.5772/intechopen.84360
[5] Cui, Yunfeng, Yongqiang Tan, Binsheng Zhao, Laura Liberman, Rakesh Parbhu, Jennifer Kaplan, Maria Theodoulou, Clifford Hudis, and Lawrence H. Schwartz. "Malignant lesion segmentation in contrast-enhanced breast MR images based on the marker-controlled watershed." *Medical physics* 36, no. 10 (2009): 4359-4369. https://doi.org/10.1118/1.3213514
[6] Dhage, Padmakant, M. R. Phegade, and S. K. Shah. "Watershed segmentation brain tumor detection." In *2015 International Conference on Pervasive Computing (ICPC)*, pp. 1-5. IEEE, 2015. https://doi.org/10.1109/PERVASIVE.2015.7086967
[7] Dhankhar, Sonika, Shobha Tyagi, and T. Prasad. "Brain MRI segmentation using K-means algorithm." In *National Conference on Advances in Knowledge Management*, pp. 1-5. 2010.
[8] Dhiman, Gaurav, Sapna Juneja, Wattana Viriyasitavat, Hamidreza Mohafez, Maryam Hadizadeh, Mohammad Aminul Islam, Ibrahim El Bayoumy, and Kamal Gulati. "A novel machine-learning-based hybrid CNN model for tumor identification in medical image processing." *Sustainability* 14, no. 3 (2022): 1447. https://doi.org/10.3390/su14031447
[9] Ding, Yuhan, Lisha Hua, and Shunlei Li. "Research on computer vision enhancement in intelligent robot based on machine learning and deep learning." *Neural Computing and Applications* (2022): 1-13.
[10] Hagler Jr, Donald J., SeanN Hatton, M. Daniela Cornejo, Carolina Makowski, Damien A. Fair, Anthony Steven Dick, Matthew T. Sutherland *et al.,* "Image processing and analysis methods for the Adolescent Brain Cognitive Development Study." *Neuroimage* 202 (2019): 116091.
[11] Hore, Alain, and Djemel Ziou. "Image quality metrics: PSNR vs. SSIM." In *2010 20th international conference on pattern recognition*, pp. 2366-2369. IEEE, 2010. https://doi.org/10.1109/ICPR.2010.579
[12] Hou, Yue, Qiuhan Li, Chen Zhang, Guoyang Lu, Zhoujing Ye, Yihan Chen, Linbing Wang, and Dandan Cao. "The state-of-the-art review on applications of intrusive sensing, image processing techniques, and machine learning methods in pavement monitoring and analysis." *Engineering* 7, no. 6 (2021): 845-856. https://doi.org/10.1016/j.eng.2020.07.030
[13] Vineela, T., R. V. G. L. Akhila, T. Anusha, Y. Nandini, and S. Bindu. "Kidney stone analysis using digital image processing." *International journal of advanced research in electrical, electronics and instrumentation engineering* 3 (2020): 001-004.
[14] Rajput, Siddharth, Abhilasha Singh, and Ritu Gupta. "Automated kidney stone detection using image processing techniques." In *2021 9th International Conference on Reliability, Infocom Technologies and Optimization (Trends and Future Directions)(ICRITO)*, pp. 1-5. IEEE, 2021. https://doi.org/10.1109/ICRITO51393.2021.9596175
[15] Akkasaligar, Prema T., Sunanda Biradar, and Veena Kumbar. "Kidney stone detection in computed tomography images." In *2017 International Conference On Smart Technologies For Smart Nation (SmartTechCon)*, pp. 353-356. IEEE, 2017. https://doi.org/10.1109/SmartTechCon.2017.8358395
[16] Cui, Yingpu, Zhaonan Sun, Shuai Ma, Weipeng Liu, Xiangpeng Wang, Xiaodong Zhang, and Xiaoying Wang. "Automatic detection and scoring of kidney stones on noncontrast CT images using STONE nephrolithometry: combined deep learning and thresholding methods." *Molecular Imaging and Biology* 23 (2021): 436-445. https://doi.org/10.1007/s11307-020-01554-0
[17] Thein, Nilar, Hanung Adi Nugroho, Teguh Bharata Adji, and Kazuhiko Hamamoto. "An image preprocessing method for kidney stone segmentation in CT scan images." In *2018 International Conference on Computer Engineering, Network and Intelligent Multimedia (CENIM)*, pp. 147-150. IEEE, 2018. https://doi.org/10.1109/CENIM.2018.8710933
[18] Elton, Daniel C., Evrim B. Turkbey, Perry J. Pickhardt, and Ronald M. Summers. "A deep learning system for automated kidney stone detection and volumetric segmentation on noncontrast CT scans." *Medical Physics* 49, no. 4 (2022): 2545-2554. https://doi.org/10.1002/mp.15518
[19] Hasan, SM Kamrul, and Mohiudding Ahmad. "Two-step verification of brain tumor segmentation using watershed-matching algorithm." *Brain informatics* 5, no. 2 (2018): 8. https://doi.org/10.1186/s40708-018-0086-x
[20] Tarhini, Ghinwa M., and Reda Shbib. "Detection of brain tumor in MRI images using watershed and threshold-based segmentation." *International Journal of Signal Processing Systems* 8, no. 1 (2020): 19-25. https://doi.org/10.18178/ijsps.8.1.19-25
[21] Khan, Muhammad A., Ikram U. Lali, Amjad Rehman, Mubashar Ishaq, Muhammad Sharif, Tanzila Saba, Saliha Zahoor, and Tallha Akram. "Brain tumor detection and classification: A framework of marker-based watershed

algorithm and multilevel priority features selection." *Microscopy research and technique* 82, no. 6 (2019): 909-922. https://doi.org/10.1002/jemt.23238

[22] Seere, Santhosh Kumar Hatcholli, and K. Karibasappa. "Threshold segmentation and watershed segmentation algorithm for brain tumor detection using support vector machine." *European Journal of Engineering and Technology Research* 5, no. 4 (2020): 516-519. https://doi.org/10.24018/ejeng.2020.5.4.1902

[23] Jemimma, T. A., and Y. Jacob Vetharaj. "Watershed algorithm based DAPP features for brain tumor segmentation and classification." In *2018 International Conference on Smart Systems and Inventive Technology (ICSSIT)*, pp. 155-158. IEEE, 2018. https://doi.org/10.1109/ICSSIT.2018.8748436

[24] Baygin, Mehmet, Orhan Yaman, Prabal Datta Barua, Sengul Dogan, Turker Tuncer, and U. Rajendra Acharya. "Exemplar Darknet19 feature generation technique for automated kidney stone detection with coronal CT images." *Artificial Intelligence in Medicine* 127 (2022): 102274. https://doi.org/10.1016/j.artmed.2022.102274

[25] Kaplan, Ela, Mehmet Baygin, Prabal D. Barua, Sengul Dogan, Turker Tuncer, Erman Altunisik, Elizabeth Emma Palmer, and U. Rajendra Acharya. "ExHiF: Alzheimer's disease detection using exemplar histogram-based features with CT and MR images." *Medical Engineering & Physics* 115 (2023): 103971. https://doi.org/10.1016/j.medengphy.2023.103971

[26] Sut, Suat Kamil, Mustafa Koc, Gokhan Zorlu, Ihsan Serhatlioglu, Prabal Datta Barua, Sengul Dogan, Mehmet Baygin, Turker Tuncer, Ru-San Tan, and U. Rajendra Acharya. "Automated Adrenal Gland Disease Classes Using Patch-Based Center Symmetric Local Binary Pattern Technique with CT Images." *Journal of Digital Imaging* (2023): 1-14. https://doi.org/10.1007/s10278-022-00759-9

[27] Tuncer, Ilknur, Prabal Datta Barua, Sengul Dogan, Mehmet Baygin, Turker Tuncer, Ru-San Tan, Chai Hong Yeong, and U. Rajendra Acharya. "Swin-textural: A novel textural features-based image classification model for COVID-19 detection on chest computed tomography." *Informatics in Medicine Unlocked* 36 (2023): 101158. https://doi.org/10.1016/j.imu.2022.101158

[28] Pandey, Mohit, and Abhishek Gupta. "Tumorous kidney segmentation in abdominal CT images using active contour and 3D-UNet." *Irish Journal of Medical Science (1971-)* 192, no. 3 (2023): 1401-1409. https://doi.org/10.1007/s11845-022-03113-8

[29] Pandey, Mohit, and Abhishek Gupta. "A systematic review of the automatic kidney segmentation methods in abdominal images." *Biocybernetics and Biomedical Engineering* 41, no. 4 (2021): 1601-1628. https://doi.org/10.1016/j.bbe.2021.10.006

[30] Pandey, Mohit, and Abhishek Gupta. "An approach to remove extraneous slices from CT for kidney segmentation." In *2022 1st IEEE International Conference on Industrial Electronics: Developments & Applications (ICIDeA)*, pp. 116-121. IEEE, 2022. https://doi.org/10.1109/ICIDeA53933.2022.9970062